Geomechanics and Engineering, *Vol. 14, No. 5 (2018) 439-451*
DOI: https://doi.org/10.12989/gae.2018.14.5.439

Study of stability and evolution indexes of gobs under unloading effect in the deep mines

Jianxin Fu[1,2], Wei-Dong Song[*1] and Yu-Ye Tan[1a]

[1]*School of Civil and Resource Engineering, University of Science and Technology Beijing, Beijing 100083, China*
[2]*School of Engineering, University of Tokyo, Tokyo 110-0008, Japan*

(Received July 29, 2016, Revised August 8, 2017, Accepted August 19, 2017)

Abstract. The stress path characteristics of surrounding rock in the formation of gob were analysed and the unloading was solved. Taking Chengchao Iron Mine as the engineering background, the model for analysing the instability of deep gob was established based on the mechanism of stress relief in deep mining. The energy evolution law was investigated by introducing the local energy release rate index (LERR), and the energy criterion of instability of surrounding rock was established based on the cusp catastrophe theory. The results showed that the evolution equation of the local energy release energy of the surrounding rock was quartic function with one unknown and the release rate increased gradually during the mining. The calculation results showed that the gob was stable. The LERR per unit volume of the bottom structure was relatively smaller, which mean the stability was better. The LERR distribution showed that there was main energy release in the horizontal direction and energy concentration in the vertical direction which meet the characteristics of deep mining. In summary, this model could effectively calculate the stability of surrounding rock in the formation of gob. The LERR could reflect the dynamic process of energy release, transfer and dissipation which provided an important reference for the study of the stability of deep mined out area.

Keywords: deep mine; gob; unloading; local energy release rate; cusp catastrophe

1. Introduction

Underground mining is the main method to gain metal mineral resources. In the process of mining, the ore is excavated from the ore body by mechanical cutting or blasting technology, and the hollow areas formed in the ore body are called gob, or mined out area, or goaf (Mine Safety Terms 2008). At present, the mining scale of China has ranked the first in the world, and there are 20,000 coal mines, more than 10,000 underground metal mines. The total ore production per year reaches 5 billion tons and the volume of new gob per year is about 150 million cubic meters (Ma, 2012).

Analysis of gob stability is always the hot topic of mine safety research, and also an extremely complex problem, especially in deep mines (Anon 1986, Sakamoto *et al.* 2005). The methods of stability analysis mainly include theoretical analysis, prediction evaluation, physical model test and numerical simulation (Whittles *et al.* 2007, Srisharan 2016).

Theoretical analysis method was used to analyze the stability of gob in the early stage. Based on the actual situation, the structure of gob is simplified as an ideal mechanical model which composed by pillar and roof (Hoek 1980). Then, the stability of roof and pillar is analyzed through the elastoplastic theory, such as beam theories (Please 2013), plates and shells theories (He 2007), elastic foundation beam theory (An 2016), viscoelastic-plastic creep theories (Wang 2016) and so on. However, much simplification has been carried out in the theoretical analysis and the in-situ stress is not considered, which causes the analysis results are not consistent with the actual situation.

In the analysis process of prediction evaluation, the influence factors of gob stability are determined by the analysis of similar engineering cases, and the evaluation model is established to evaluate and predict the stability of gobs. Overall, the common methods include uncertainty measurement theory (Gone 2008), fuzzy mathematics theory (Tao 2016), artificial neural network (Lai 2003), support vector machine (Wang 2015) and so on. However, the prediction evaluation method is qualitative or semi quantitative, whose results are not universal. The stress change of surrounding rock cannot be obtained.

The physical model test method can be used to show the change law of stress, displacement and fracture in details through constructing a model similar to the actual project. Physical model test has been widely used in various engineering fields, and become an important method to solve complex engineering problems (Hancock 2004, Chen 2006). However, this method is difficult and the in-situ stress cannot be stimulated. Therefore, the results are also not consistent with the actual situation.

Since the development of numerical calculation and computer performance, the numerical simulation has become the most widely used method (Mote 1971, Terada 2001, Wang 2011). Numerical simulation method can

∗Corresponding author, Professor
E-mail: songwd2004@126.com
[a]Associate Professor
E-mail: fujun-zuihao@163.com

Copyright © 2018 Techno-Press, Ltd.

ISSN: 2005-307X (Print), 2092-6219 (Online)

realize the simulation of real scene which includes in-situ stress, change of stress and displacement (Mamtimin and Rahmatjan 2014, Okada *et al.* 2005, Ouria *et al.* 2016). Therefore, the results agree well with field practice situation. More and more scholars have studied the gob stability using numerical stimulation mainly including the methods of finite element (Tulu 2011, Kripakov 1995, Chen 2010), finite difference (Song 2012, Tang 2012, Yu 2016) and discrete element (Wu 2010, Pan 2012). Among them, the finite difference method is the earliest and most widely used. The explicit finite difference is one of the most efficient methods in computing, which has been applied in the software of FLAC3D. The FLAC3D can well simulate the mechanical properties when the rock failed, which has been widely used in the mining engineering.

However, the consideration of stress change of existing researches is not complete. Rock masses underground are under a true-triaxial stress equilibrium state before mining, and a large amount of energy is gathered in the rock. In fact, the formation of gob is accompanied by the release and transfer of the stress in a certain direction. The stress state of rock changes dramatically from three-dimensional to two-dimensional even uniaxial state. When the change of stress exceeds the rock strength, the gob will destabilize. The gob instability is caused by stress release which is called unloading (Li 2014, Feng 2015).

The mechanical properties of rocks under the unloading conditions are very different from that under the loading conditions which mainly manifested as: (1) decrease of mechanical parameters; (2) deformation intensifies and (3) burst of destruction. Because of these differences above, the stability analysis of gobs based on the loading theory is inconsistent with the actual situation.

With the increases of mining depth, due to the rapid growth of stress and the complexity of occurrence environment, the instability mechanism and the stability characteristics of gob would be significantly different.

Firstly, the damage form of rock transforms gradually from brittle fracture to ductile fracture, caused the gob could maintain stable after larger deformation of rock. It means that the stable standards of gob in the shallow are no longer suitable for the gob in the deep.

Secondly, the stability of gob in the shallow is analyzed and evaluated using stress, strain, plastic zone and so on, but after entering into the deep, there is a large amount of elastic energy gathered in the rock due to the high pressure. The mining will cause a sharp energy release which will cause instant burst of rock, but stress is less than the rock strength. So the traditional indicators are not suitable for evaluation of rock stability. It is necessary to introduce new research indicators to accurately get the stability mechanism and characteristics of gob.

At present, the study of rock stability evaluation of deep mine in South Africa ranks the world leader. In South Africa, many years of theoretical researches and practices have shown that the energy release rate is a suitable indicator of stability evaluation of rock in the deep mines.

Above all, based on published researches, considering the actual stress variation in the process of deep mining, the numerical calculation model of deep stope under unloading affect was established to investigate the geotechnical behavior and the stability of deep stope under a high in-situ stress condition in Chengchao Iron Mine in China. Moreover, the stability discrimination model of deep stope based on the cusp catastrophe theory was established. The change characteristics of stress field and the distribution and extension of the plastic zone were studied based on the results of numerical simulation. In addition, the energy evolution was analyzed by introducing the local energy release rate index (LERR), and the energy criterion of the rock instability was established based on the cusp catastrophe theory. In order to examine the validity of the model and the parameters, we compared the numerical analyses results with the deformation monitoring data obtained from the field.

2. Unloading process during the formation of gob and numerical method

2.1 Process and calculation of unloading

Underground mining is actually a process of unloading. It can be seen from rock mechanics experimental test results that rock strength is often higher under the triaxial loading, but the unloading causes the rapid deterioration of the rock strength. In general, the stress change includes loading and unloading in the process of underground mining. The stress state of surrounding rock is shown in Fig. 1.

Actually, the formation of gob is the process of appearance and disappearance of unbalanced force, so the unloading force is a kind of unbalanced force. The unloading force can be obtained by computing the unbalanced force. The unloading force is the nodal unbalanced force in the finite element method. Taking the triangular element as an example, the force of each nodal is shown in Fig. 2.

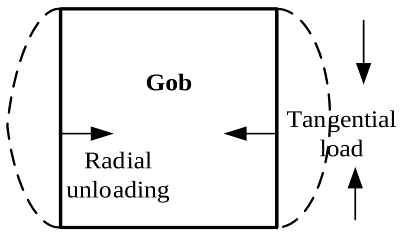

Fig. 1 The stress state of surrounding rock during the formation of gob

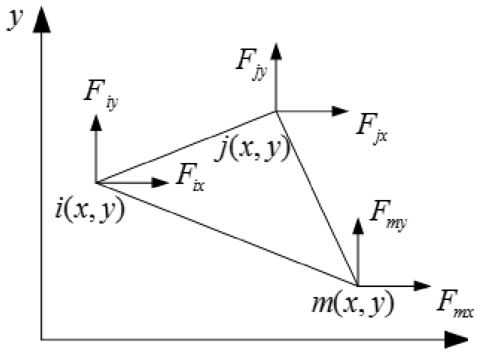

Fig. 2 Force diagrams of triangular element

The force of triangular nodal satisfies the relationship which can be expressed as

$$\{F\}_e = \{F_{ix}, F_{iy}, F_{jx}, F_{jy}, F_{mx}, F_{my}\}^T = [K]_e\{\delta\}_e \tag{1}$$

where $\{F\}_e$ is the nodal force, $[K]_e$ is the element stiffness matrix.

Then, based on the elastic mechanics, the following formula can be obtained as

$$[K]_e\{\delta\}_e = t \cdot \Delta_e \cdot [B]^T \cdot [D] \cdot [B]\{\delta\}_e = t \cdot \Delta_e \cdot [B]^T \cdot [S]\{\delta\}_e = t \cdot \Delta_e \cdot [B]^T\{\sigma\}_e \tag{2}$$

where Δ_e is the area of the triangle which can be expressed as

$$\Delta_e = \frac{1}{2}\begin{bmatrix} 1 & x_i & y_i \\ 1 & x_j & y_j \\ 1 & x_m & y_m \end{bmatrix} \tag{3}$$

where $[D]$ is element elasticity matrix and $[B]$ is geometric matrix. They can be expressed as

$$[D] = \frac{E}{1-\mu^2}\begin{bmatrix} 1 & \mu & 0 \\ \mu & 1 & 0 \\ 0 & 0 & \frac{1-\mu}{2} \end{bmatrix}$$
$$[B] = \frac{1}{2\Delta_e}\begin{vmatrix} b_i & 0 & b_j & 0 & b_m & 0 \\ 0 & c_i & 0 & c_j & 0 & b_m \\ c_i & b_i & c_j & b_j & c_m & b_m \end{vmatrix} \tag{4}$$

in which, E is rock elastic modulus and μ is Poisson ratio. Other parameters satisfy the following relationships which can be expressed as

$$b_i = y_j - y_m, \quad b_j = y_m - y_i, \quad b_m = y_i - y_j,$$
$$c_i = x_m - y_j, \quad c_j = x_i - x_m, \quad c_m = x_j - x_i \tag{5}$$

Assumed the element stress on the center of gravity is $\{\sigma\}_e$ which can be expressed as

$$\{\sigma\}_e = \{\sigma_x, \sigma_y, \tau_z\}^T \tag{6}$$

Substituting the formula (5) and (4) into the formula (2) can be obtained as

$$[F_{ix}, F_{iy}, F_{jx}, F_{jy}, F_{mx}, F_{my}]^T = t \cdot \begin{bmatrix} b_i & 0 & b_j & 0 & b_m & 0 \\ 0 & c_i & 0 & c_j & 0 & c_m \\ c_i & b_i & c_j & b_j & c_m & b_m \end{bmatrix} \cdot \begin{pmatrix} \sigma_x \\ \sigma_y \\ \tau_z \end{pmatrix} \tag{7}$$

Adding all the nodal force together, the unbalanced force can be obtained as

$$F_{sx} = \sum_e F_{sx}^e, \quad F_{sy} = \sum_e F_{sy}^e \tag{8}$$

Obviously, the sum of nodal force of the unexploited region is zero while the sum of nodal force on the boundary of mining region is not zero. It means that unbalanced force appears and it is the unloading force on the mining region boundary.

2.2 Numerical simulation of unloading

A computer program was developed based on the methods in the previous section. The calculation procedures include the following steps:

(1) To build the model containing the mining area, then to mesh the model. The mining area can be meshed fine and modeled independently according to mining sequence.

(2) To apply the stress and displacement boundary conditions and initialize the ground stress, then to calculate the initial nodal stress (σ_0) of elements.

(3) To mine the ore in the mining region and calculate all the nodal stress (σ'). Before carrying out the addition operation, the mining disturbed zone (MDZ) should be determined. The stress and displacement of nodal in the MDZ are added together. Then the unloading stress and displacement are obtained as

$$\sigma_1 = \sigma_0 + \sigma' \tag{9}$$

There are generally many mining steps which mean multiple calculation of unloading. The unloading stress of any step is the previous nodal stress coupled with the nodal stress which can be expressed as

$$\sigma_i = \sigma_{i-1} + \sigma'_i \tag{10}$$

After getting the unloading stress, the displacement of corresponding nodal need to be calculated. In order to reduce the computational difficulty, unloading is assumed to have no impact on the rock mechanic parameters. The flow of modeling and calculating is shown in Fig. 3.

3. Analysis of stability and indexes of deep gob

The instability of underground gob mainly includes the following aspects:

(1) Due to the stress release in the middle of roof and pillar, the tensile failure will occur in these positions；

(2) Because of the stress concentration, the compressive shear failure will occur in the corner and the lower part of the pillar;

(3) The slip and shear failure along with the structural plane will occur in local surrounding rock.

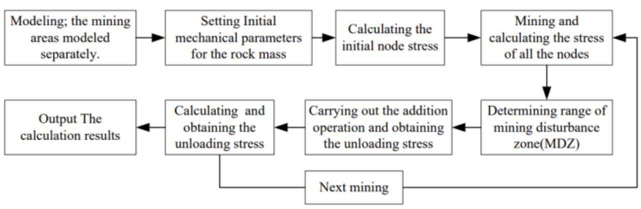

Fig. 3 The flow diagram of modeling and calculation

However, the mechanical properties of rock have obviously changed under the action of high stress, and the stability characteristics of the gob also have changed greatly. A large number of engineering examples have shown that the stress does not reach the peak strength of rock when the gob is unstable, so it is not enough to consider only the stress index. Under the action of high stress, a large amount of elastic energy is gathered inside the rock, and the mining will cause the sharp release of energy which is very different from the stress. Therefore, it is necessary to consider the evolution law of energy so that the stability mechanism of deep gob can be studied comprehensively and systematically.

3.1 Energy release law of surrounding rock during the formation process of gob

There are generally many mining steps during the formation of gob. Assumed the volume of gob of each mining is dV, the energy released is dW_r, energy release rate (ERR) can be calculated as

$$ERR = \frac{dW_r}{dV} \tag{11}$$

When the formation of gob after m steps of mining, the average energy release rate can be expressed as

$$\overline{ERR} = \frac{\sum_{i=1}^{m} ERR_i}{m} \tag{12}$$

The ERR can reflect the energy release law of surrounding rock of different mining steps and the influences on the stability of gob.

But a lot of studies and engineering examples have shown that the gob instability in the deep mines is often caused by the sharp release of internal elastic energy which usually happens at the local position. Although the traditional energy release index can reflect the energy change of surrounding rock, it cannot reflect the sudden instability of surrounding rock. Therefore, the local energy release rate index (LERR) (Su 2006) is introduced in this paper to study the instability law of gob.

The local energy release rate index (LERR) can characterize the strain energy change of local position of rock before and after failure. It is the difference value between the elastic energy density of elements before and after failure. It can be calculated as

$$LERR_i = ESED_{i\max} - ESED_{i\min} \tag{13}$$

where $LERR_i$ is the local energy release rate of element i; $ESED_{imax}$ is the maximum value of elastic strain energy density of element i before failure, $ESED_{imin}$ is the minimum value of elastic strain energy density of element i after failure.

So the total local elastic energy release (LEER) of the failure elements can be expressed as

$$LEER = \sum_{i=1}^{n} (LERR_i \; V_i) \tag{14}$$

where V_i is the volume of the failure elements. The $ESED_{imax}$ and $ESED_{imin}$ are expressed as

$$ESED_{i\max} = [\sigma_1^2 + \sigma_2^2 + \sigma_3^2 - 2\mu(\sigma_1\sigma_2 + \sigma_1\sigma_3 + \sigma_2\sigma_3)]/2E \tag{15}$$

$$ESED_{i\min} = [\sigma_1'^2 + \sigma_2'^2 + \sigma_3'^2 - 2\mu(\sigma_1'\sigma_2' + \sigma_1'\sigma_3' + \sigma_2'\sigma_3')]/2E \tag{16}$$

where σ_1, σ_2, σ_3 are the principal stress before the failure of elements; σ'_1, σ'_2, σ'_3 are the principal stress after the failure of elements, μ is Poisson ratio and the E is elastic modulus.

3.2 The cusp catastrophe model of local elastic energy

Mutation theory is firstly proposed by Thom that is an effective tool to study the phenomenon of jumping instability. The cusp catastrophe theory is the most common mutation theory. It has been widely used in the stability analysis of mine.

For the equilibrium problem in three dimensional spaces, 1 state variable and 2 control variables are included the standard equation of the cusp catastrophe model is expressed as

$$V(x) = x^4 + ux^2 + vx \tag{17}$$

where u and v are control variables, x is state variable.

It can also be called the potential function of the system stable variable, When the potential function satisfies the following conditions which is expressed in the formula 18, the system is stable.

$$V'(x) = 4x^3 + 2ux + v = 0 \tag{18}$$

The singular point equation can be obtained as

$$V''(x) = 12x^2 + 2u = 0 \tag{19}$$

Then, the discriminant of the system stability is expressed as

$$\Delta = 8u^3 + 27v^2 \tag{20}$$

When $\Delta=0$, the system is in a critical state of equilibrium; when $\Delta<0$, the system is unstable; when $\Delta>0$, the system is stable.

It can be known from the above analysis that the local elastic energy of any failure element i of mining step n can be expressed as

$$LEER(n) = LERR_i(n) \times V_i \tag{21}$$

where LEER is the local elastic energy of mining step n.

Because numbers of failure elements of different mining step are different, so the corresponding LEER are also different. The sequence of LEER data can be obtained as

$$\{LEER\} = \{LEER(1),\; LEER(2)......,\; LEER(n)\}$$

The LEER data are polynomial fitted to get the function relationship between LEER and the mining steps which can be expressed as $LEER=f(n)$ and its Taylor expansion can be obtained as

$$LEER = f(n) = f(0) + \left.\frac{\partial f}{\partial n}\right|_{n=0} \times n + \left.\frac{\partial^2 f}{\partial n^2}\right|_{n=0} \times n^2 + \ldots + \left.\frac{\partial^k f}{\partial n^k}\right|_{n=0} \times n^k + \ldots \tag{22}$$

To reserve the first four of Taylor expansion and the expressions can be expressed as

$$LEER = \sum_{i=0}^{4} \frac{\partial f}{\partial n^{i}} \times n^{i} \tag{23}$$

Set $\frac{\partial f}{\partial n^{i}} = a_i$, then the LEER can be expressed as

$$LEER = a_0 + a_1 n + a_2 n^2 + a_3 n^3 + a_4 n^4 \tag{24}$$

To set $n = x - \frac{a_3}{4a_4} = x - L$, then the LEER can be expressed as

$$LEER = b_0 + b_1 x + b_2 x^2 + b_4 x^4 \tag{25}$$

where

$$L = \frac{a_3}{4a_4}, \quad \begin{bmatrix} b_0 \\ b_1 \\ b_2 \\ b_4 \end{bmatrix} = \begin{bmatrix} 1 & L & L^2 & 3L^4 \\ 0 & 1 & 2L & 8L^3 \\ 0 & 0 & 1 & 6L^2 \\ 0 & 0 & 0 & 8L^3 \end{bmatrix} \begin{bmatrix} a_0 \\ a_1 \\ a_2 \\ a_4 \end{bmatrix}.$$

To transform the formula (25), the following expressions can be obtained as

$$\frac{LEER}{b_4} = \frac{b_0}{b_4} + \frac{b_1}{b_4} x + \frac{b_2}{b_4} x^2 + x^4 \tag{26}$$

If the constant term is ignored, the LEER can be expressed as

$$LEER = x^4 + \left(\frac{a_2}{a_4} - \frac{3a_3^2}{8a_4^2}\right)x^2 + \left(\frac{a_1}{a_4} - \frac{a_2 a_3}{2a_4^2} + \frac{a_3^3}{8a_4^3}\right)x \tag{27}$$

Finally, the cusp catastrophe model of local elastic energy is obtained as

$$\Delta = 8u^3 + 27v^2 = 8\left(\frac{a_2}{a_4} - \frac{3a_3^2}{8a_4^2}\right)^3 + 27\left(\frac{a_1}{a_4} - \frac{a_2 a_3}{2a_4^2} + \frac{a_3^3}{8a_4^3}\right)^2 \tag{28}$$

When Δ=0, the gob is in a critical state of equilibrium; when Δ<0, the gob is unstable; when Δ>0, the gob is stable. Where a_i is constant which can be determined by polynomial fitting.

2.3 Stability analysis index for the deep gob

Above all, five indexes are selected which include the following aspects:

(1) The stress field;

(2) Volume and the range of plastic zone;

(3) The local energy release rate index (LERR) is used to analyze the energy evolution of key zones;

(4) The total local elastic energy release (LEER) is used as the index of the damage degree of rock.

(5) The cusp catastrophe model and discriminant value are used to analyze the stability degree.

Considering the above 5 factors, the whole gob and the key zones of gob can be studied comprehensively.

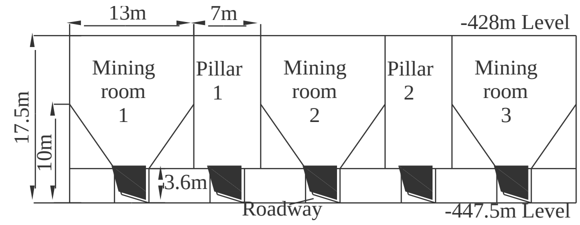

Fig. 4 The schematic diagram of mining method

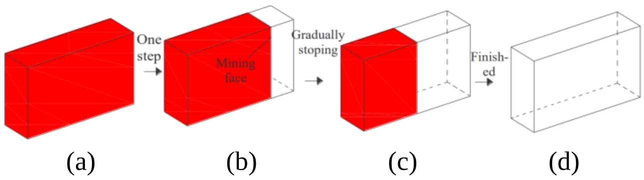

Fig. 5 The schematic diagram of formation processes of gob, (a) Before mining formation process, (b) Started forming, (c) Formation process and (d) Finishing

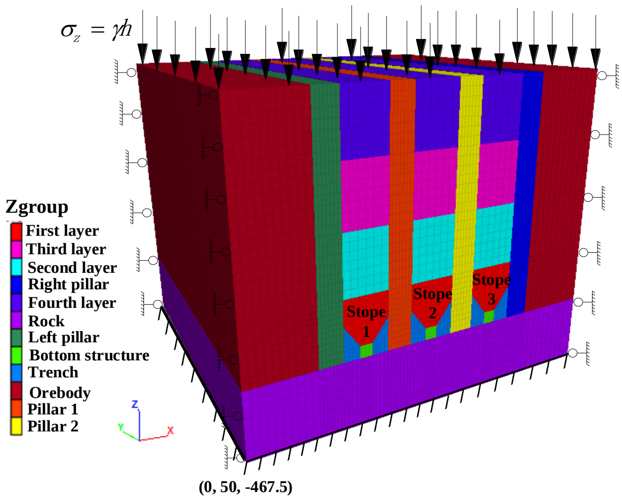

Fig. 6 The diagram of stimulate model

Table 1 Mechanical and deformation parameters

Rock types	Uniaxial compressive strength (MPa)	Uniaxial tensile strength (MPa)	Cohesion (MPa)	Internal friction angle (°)	Elastic Modulus (GPa)	Poisson's ratio
Iron	49.85	5.55	8.32	33.6	14.96	0.31
Granite	65.77	3.81	6.15	36.2	9.44	0.27

4. Applications in the stability of deep gob

4.1 Engineering Background

The mining depth of Chengchao Iron Mine has reached 700 m and the main mining level is -430 m. To control the movement of ground surface, sublevel open stope mining followed by filling method is taken as the main mining method below -500 m level. In order to accumulate engineering experience, a special ore section is selected as the region of mining experiment.

The schematic diagram of this mining method is shown in Fig. 4. The ore should be divided into mining rooms and pillars and the rooms and pillars are alternatively mined. The span of the mining room is 13 m and the width of the pillar is 7 m. The length of the room and the pillar is 40 m.

The retreating mining is used and the length of one mining step is 4 m. The formation processes of gob are shown in Fig. 5.

The mechanics and deformation parameters are shown in the Table 1.

4.2 Construction of numerical model

Based on the above analysis, the three dimensional numerical model was constructed and shown in Fig. 6. Different parts were separately modeled. The length is 107 m, the width is 100 m and the height is 90 m.

The research emphasis of this paper is the stability law during the formation process of gob, so the pillar mining and filling process are not stimulated. Only the first layer mining is stimulated.

4.3 Boundary condition

The in-situ stress was obtained by applying the overcoring technique using KX-81 triaxial hollow inclusion stress gauge. The results showed that maximum horizontal principal stress is $\sigma_1 = 1.60\gamma h$, intermediate principal stress is $\sigma_2 = \gamma h$, minimum horizontal principal stress is $\sigma_3 = 0.39\gamma h$. Where, γ is the rock bulk density, h is the height of rocks.

The direction of maximum horizontal principle stress is N75°W. Note that in the FLAC3D analyses, the maximum and minimum in situ stress directions are set up in X and Y directions, respectively. The vertical stress applied at the top boundary (at a depth of 590 m) of the model is 17.91 MPa (zz-stress in FLAC3D), a maximum horizontal principal stress of 28.65 MPa (*yy*-stress in FLAC3D) was applied in the horizontal direction along the stope axis, a minimum horizontal principal stress of 6.98 MPa (*xx*-stress in FLAC3D) was applied in the horizontal on the stope cross sectional plane.

The velocity was set to zero in X and Y directions on both side boundaries of the whole model (equivalent to no horizontal movements in X and Y directions). On the bottom boundary, the velocity was set to zero in the vertical direction (equivalent to no vertical movement). In situ *zz*-stress was increased from the top of the model to the bottom of the model according to the gravitational loading associated with the different strata in the model. The in situ xx-stress and *yy*-stress was increased from the top of the model to the bottom of the model according to the gravitational loading and the lateral earth pressure coefficients in the *x*- and *y*-directions, respectively.

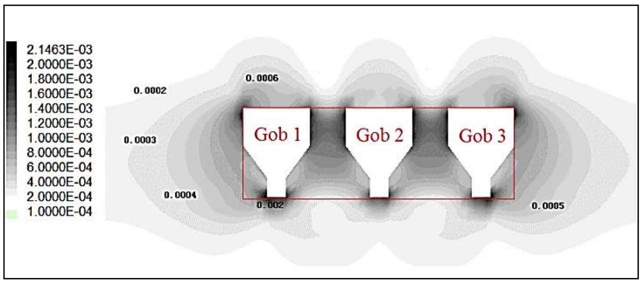

Fig. 7 The contour plot of volume strain

4.4 Determination of the boundary of unloading zone

Before the stimulation, the unloading zone should be determined. The tensile-shear failure is the important form of unloading failure of rock, so the shear deformation should be concerned. The deformation of elastoplastic continuous medium is usually divided into two types which are volume deformation and shear deformation. It can be expressed as

$$\varepsilon_{ij} = \begin{vmatrix} \varepsilon_m & 0 & 0 \\ 0 & \varepsilon_m & 0 \\ 0 & 0 & \varepsilon_m \end{vmatrix} + \begin{vmatrix} \varepsilon_x - \varepsilon_m & \frac{1}{2}\gamma_{xy} & \frac{1}{2}\gamma_{xz} \\ \frac{1}{2}\gamma_{yx} & \varepsilon_y - \varepsilon_m & \frac{1}{2}\gamma_{yz} \\ \frac{1}{2}\gamma_{zx} & \frac{1}{2}\gamma_{zy} & \varepsilon_z - \varepsilon_m \end{vmatrix} \tag{29}$$

The shear deformation can be expressed by the second invariant of deviatoric tensor of strain. They are:

Shear strain of octahedral: $\tau_8 = \frac{2\sqrt{2}}{3}\sqrt{J_2^{'}}$. Generalized shear strain: $\bar{\tau} = \frac{2}{\sqrt{3}}\sqrt{J_2^{'}}$. Pure shear strain: $\tau_s = 2\sqrt{J_2^{'}}$, where

$$J_2^{'} = \frac{1}{6}[(\varepsilon_x \text{-} \varepsilon_y)^2 + (\varepsilon_y \text{-} \varepsilon_z)^2 + (\varepsilon_x \text{-} \varepsilon_z)^2] + \frac{3}{2}(\tau_{xy}^2 + \tau_{xz}^2 + \tau_{yz}^2)$$

Comprehensively considering the characteristics of the various types of shear strain, $\tau^{'} = \sqrt{J_2^{'}}$ is used as the critical value of MDZ. The distribution contour of shear strain is shown in Fig. 7.

There are obvious zoned phenomena in the distribution of shear strain after mining. Based on the shear strain value in Fig. 7, the value of 1×10^{-4} can be taken as the critical value of MDZ and the value of 2×10^{-4} can be taken as the critical value of unloading affected zone. The automatic identification of MDZ can be realized by writing targeted program using FISH language of the FLAC3D.

5. Results and discussion

5.1 Analysis of stress field

The length of each stope is 40 m, which starting at y=80 m and ending at y=120 m. The section plane is cut at the position of y=100, which is as shown in Fig. 8. When the analysis is carried out, every index on the cutting plane will be focused on.

(1) The maximum principle stress

As shown in Fig. 9 it is the maximum principle stress. from Fig. 9, it can be know that after the formation of gobs, there is obvious stress release in trench of every gob. There is obvious stress concentration in the corner of the gob 1 and 3 whose degree is greater than that of the gob 2. The maximum value appears in the left corner of bottom structure of gob 1 which is 58.7 MPa, and the stress concentration factor is 2.26. The minimum value appears in

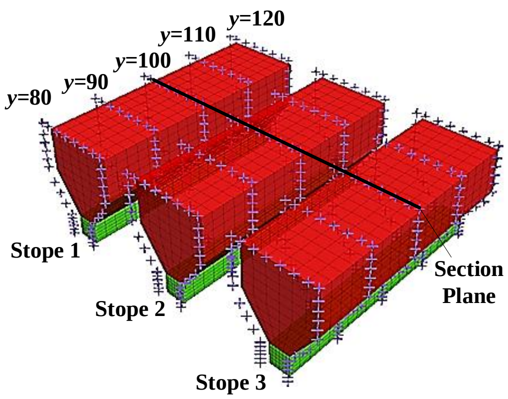

Fig. 8 Schematic diagram of stope size and section plane

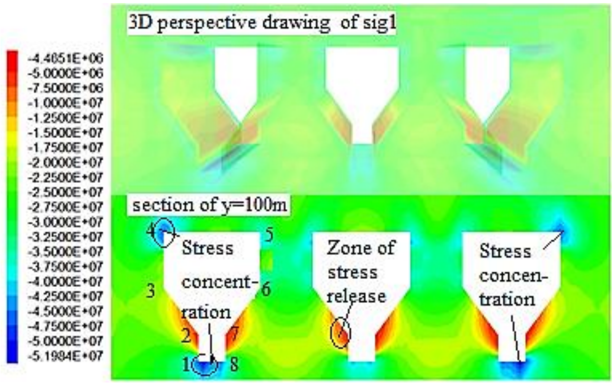

Fig. 9 Maximum principal stress contour of section of y=100

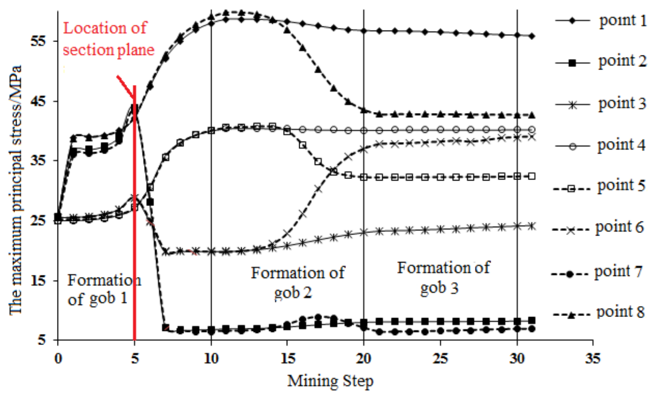

Fig. 10 Stress change curves of different points in gob 1

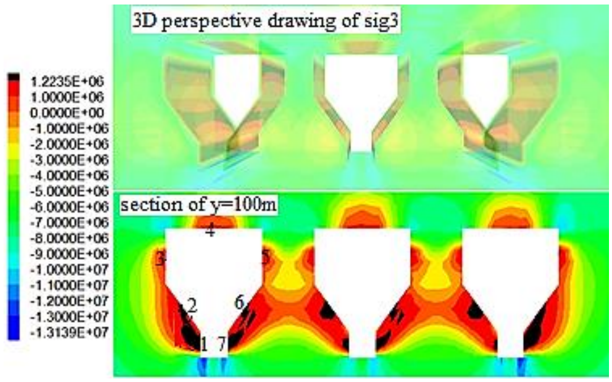

Fig. 11 Minimum principal stress contour of section plane

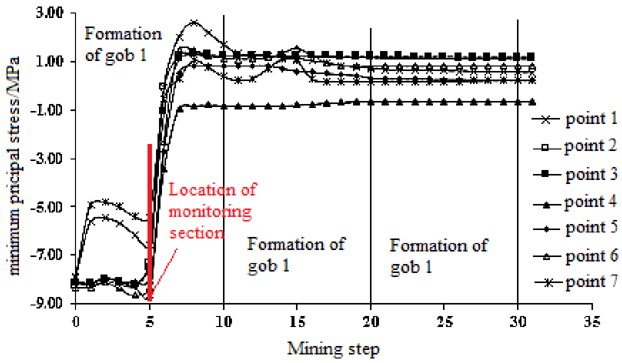

Fig. 12 Minimum principal stress curve of different points

the right side of trench of gob 2 which is 4.89MPa, and the stress release coefficient is 5.265.

In order to get the stress change during the formation of gobs, 8 points are selected and the stress change of which will be focused on. As shown in Fig. 10, it is the stress change curves of different points during the formation of gobs. It is to be noted that, in Fig. 10 the axis of abscissa indicates the mining step, and one step is equivalent to 4 m.

It can be seen from Fig. 10 that, when the distance between the section plane and the mining face is more than 4m, the stress almost remains unchanged. After the distance of the section and the mining face is 4 m, the stress increases rapidly. After the mining face gets over the section plane, the stress begins to differentiate, the stress of points 1,4,5 and 8 continues to grow while the stress of points 2,7,3,6 decreases rapidly.

Before the mining face in the stope 2 reaches the position of y=100 m, the stress remains unchanged. After the distance of the section plane and the mining face reaches 4 m, the stress of points 5 and 8 decreases obviously while the stress of point 6 increases rapidly, and the stress of point 7 increases a little. The stress of others almost remains unchanged. After the mining face in the stope 2 reaches the position of y=108 m, the stress changes slowly and the stress of point 7 decreases a little. When the stope 3 is mined, the stress of all points almost has no change.

(2) The minimum principle stress

As shown in Fig. 11, it is the contour of minimum principle stress on the section plane. From Fig. 11, it can be seen that extensive tensile stress areas appear in the trenches, the middle of roofs and pillars. The tensile stress area is more lager than that of the others. 7 points are selected in the gob, the stress of which is focused on. The minimum principal stress curves of different points are shown in Fig. 12.

The axis of abscissa is the same as that in Fig. 10. Negative value in Fig. 12 represents the compressive stress, and the positive value represents the tensile stress.

It can be seen from Fig. 12 that the stress change experiences three stages including concentration, rapid release and almost unchanged.

Before the mining face reaches the section plane, the stress of all points decreases which means concentrating of stress. After the mining face get over the section plane, stress of all points increases rapidly. After the mining face get over the location of y=108 m, the stress begins to decreases. After the formation of gob 1, stress of all points trend to stable, the impact of mining of gob 2 and 3 is little. At last, the stress of all points except point 4 changed from compressive stress to tensile stress, and the tensile stress of point 5 in the pillar 1 is the biggest.

5.2 Expansion law of plastic zone

The distribution and volume of plastic zones can reflect the stability of surrounding rock of different parts during the formation of gobs. Fig. 13 provides a plot of the plastic zone evolution law of surrounding rock of stope 1 during the formation of gob 1. Blocks of different colors represent plastic zone of different parts.

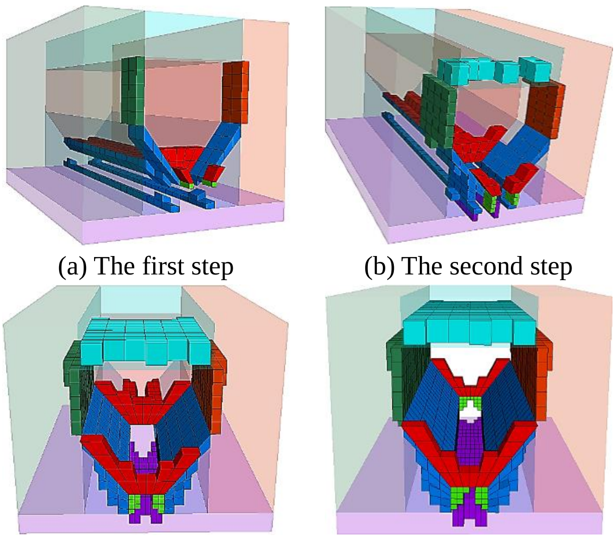
(a) The first step (b) The second step

(c) The fifth step (d) The last step

Fig. 13 Plastic zone distribution during the formation of gob 1

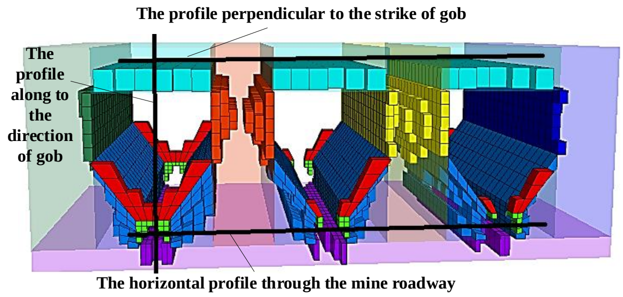

Fig. 14 Plastic zone distribution after the formation of gobs

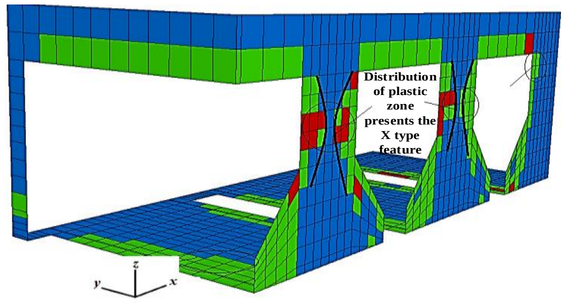

Fig. 15 Comprehensive sectional view of the distribution of plastic zone

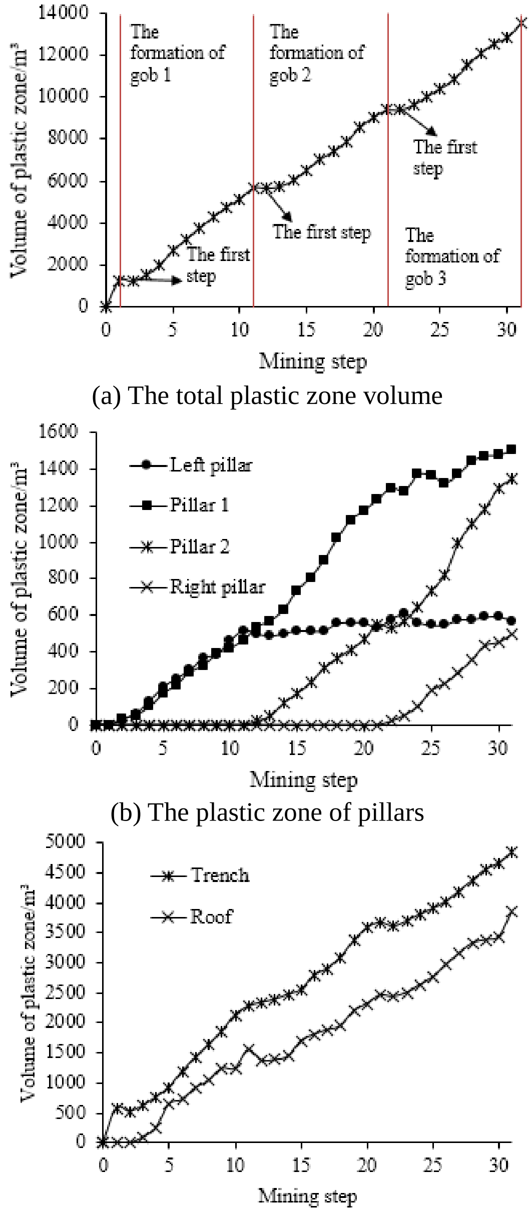

(a) The total plastic zone volume

(b) The plastic zone of pillars

(c) The plastic zone of trench and roof

Fig. 16 Change curves of plastic zone volume of different parts

After the first step mining, there is a large-scale plastic zone on the exposed surface of left pillar, pillar 1 and the trench, whose thickness is about 4m and volume is 30 m^3(shown in Fig. 13). There is also plastic zone in the mining face and the height is about 3m. However, there is no plastic zone in the roof. After the first step, the total volume of plastic zone is 1207.31 m^3.

After the second mining, the range of plastic zone of different parts increases, and there is also plastic in the roof. After the second step, the total volume of plastic zone is 1511.31 m^3, which increases 304 m^3.

With the mining, the plastic zone of surrounding rock increases continuously (shown in Fig. 13(c) and 13(d)). After the formation of gob 1, the total volume of plastic zone is 5663.75 m³. The plastic zone of left pillar is the same as that of pillar 1. The plastic zone distribution after the formation of all gobs is shown in Fig. 14, the total volume plastic zone is 13538.95 m³.

It can be seen from Fig. 14 that, after the formation of all gobs, the rocks of exposed roof surface are all in plastic damage state, the thickness of which is about 2.5 m. The plastic zone of pillar 1 and pillar 2 increases obviously, which is separately 1504 m³ and 1346.33 m³ and much larger than that of left pillar and right pillar, which increases a little. The total volume of plastic zone is 13538.95 m³. The volume of plastic zone of trench is the biggest that is 4835.52 m³. The volume of plastic zone of roof is the second biggest that is 3845.83 m³.

Three section planes are cut as shown in Fig.14, the distribution of plastic zone on the section planes is shown in Fig. 15.

From Fig. 15 we can get that the distribution of plastic of pillar 1 and 2 presents X type feature. The plastic zone distribution of trenches on the both sides is less than that of middle.

As shown in Fig. 16, they are the change curves of plastic zone volume of different parts during the formation of gobs.

It can be seen from Fig. 16 that, during the formation of gobs, the plastic zone volume of different parts increases linearly with the mining steps. The plastic zone volume decreases a little when the first step of every gob. The increasing speed of plastic zone volume in the formation of every gob is largely the same.

5.3 The change law of LERR of surrounding rock

(1) The distribution of LERR

The distributions of LERR of different mining steps are shown in Fig. 17 and the unit is J/m³. The grids in figures represent the failure rock.

It can be seen that the maximum value of LERR appears in the roof which is 2.13×10^4 $J\cdot m^{-3}$. The LERR in the corners on both sides of roof increases rapidly after the formation of the first gob and the value is 2.13×104 $J\cdot m^{-3}$. The maximum value of LERR appears in the corners of roadways of bottom structure which is 6.7×104 $J\cdot m^{-3}$. Due to the sharp release of energy, the maximum value becomes smaller which is 5.5×104 $J\cdot m^{-3}$ after formation of the second gob. The LERR of pillar 1 between the gob 1 and gob 2 increases rapidly and distribution presents X type feature which is similar with the distribution of failure rock.

The maximum value further reduces after the formation of all gobs which becomes 5.13×10^4 $J\cdot m^{-3}$. The LERR of trench grows greatly.

To select a rock element A in the trench and a rock element B in the pillar 1 and their positions are shown in Fig. 17(b).

The change curves of elastic strain energy density

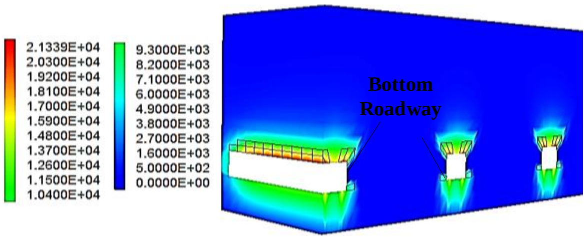

(a) After the formation of bottom structure

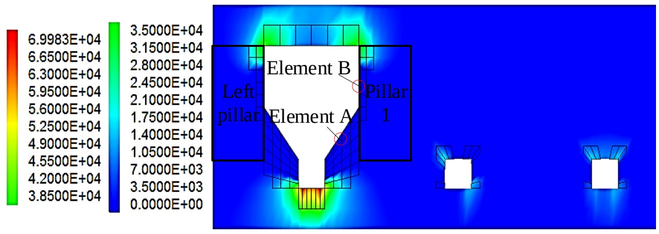

(b) After formation of the first mining room

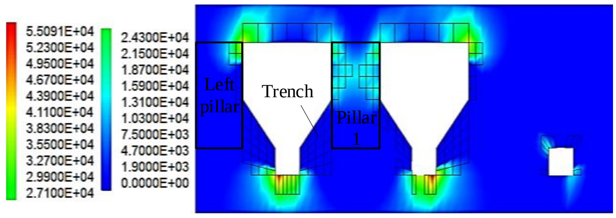

(c) After formation of the second mining room

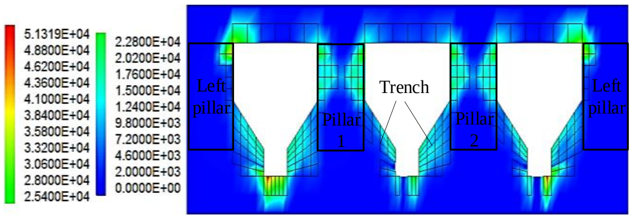

(d) After formation of all the mining room

Fig. 17 The distribution contours of rock LERR on the cross-section at y = 100 m

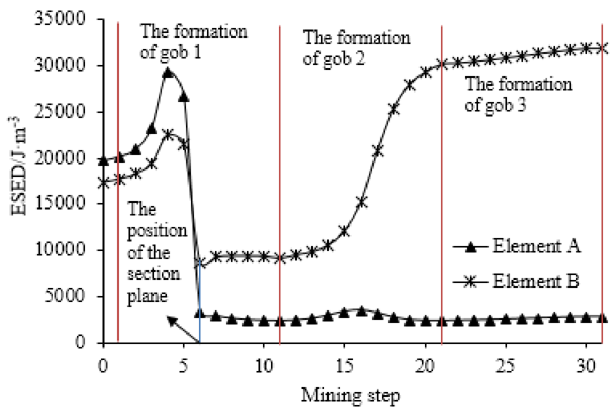

Fig. 18 The change curves of ESED of element A and B

(ESED) of element A and B during the formation of gobs are shown in Fig. 18.

It can be seen from Fig. 18 that before the mining face reaching their positions, the energy density of element A is greater than that of element B. When the mining face get over their positions, the local energy density of element A

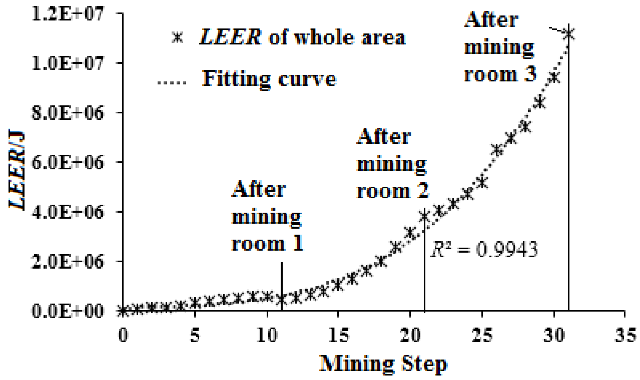

(a) The change curves of LEER of the whole areas

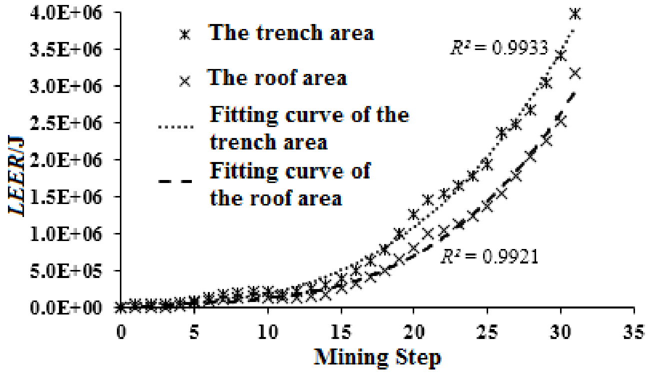

(b) The change curves of LEER of trench and roof

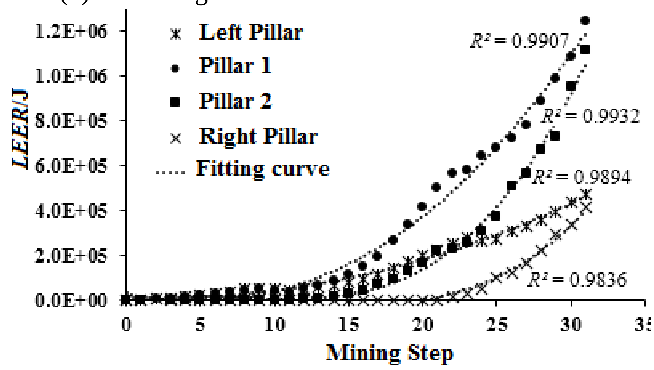

(c) The change curves of LEER of pillars

Fig. 19 The change curves of LEER of different areas

Table 2 The LEER discrimination value of key areas

Areas	a_1	a_2	a_3	a_4	△
Whole	69373	-18693.2	4447.86	-120.96	7E+07
Trench	17506	-4584	1456.44	-47.04	3.5E+07
Roof	-2417.7	3067.6	-297.06	78.72	339414
Pillar 1	2639.5	-2123.2	780.3	-46.08	172137
Pillar 2	-8698.8	2875.6	-557.58	71.04	57574.9

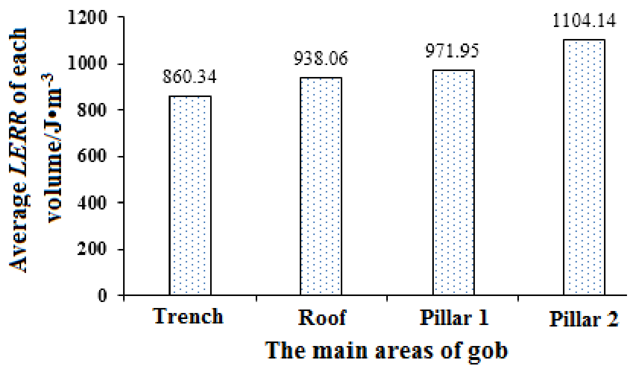

Fig. 20 The average LEER of each volume of failure elements

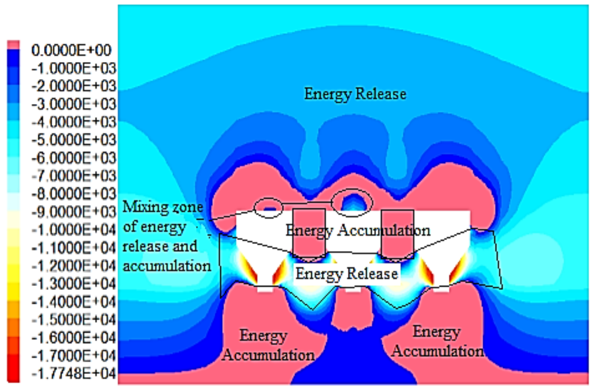

Fig. 21 The distribution of energy of cross-section

and B decrease shapely and then remain almost unchanging until the mining face in the second room reaches the positions. Then the local energy of element B in the pillar 1 increases rapidly while the local energy density of element A in the trench decreases a little. At last, the local energy density of element B is much greater than that of element A.

It can be known from above analysis that the damage degree of the element B is much higher. So the LERR index can characterize the damage degree effectively.

(2) The analysis of local elasticity energy release (LEER) of surrounding rock

The change curves of LEER of the whole areas and the key areas are shown in Fig. 19.

It can be known from Fig. 19 that the LEER of the whole and the key areas increases slowly and uniformly when mining the first room. But when the second gob is mined, the increase of LEER becomes rapid (shown in Fig. 19(a)). It is mainly because that the mining of first room causes the stress concentration and energy accumulation. But when the second gob is mined, the stress and energy release sharply which causes significantly increase of the LEER. In addition, the LEER releases more easily because the mining direction is perpendicular to the direction of maximum principal stress.

The final LEER of the trenches is greater than pillar 1 and pillar 2, because the volume of plastic zone of the trench areas is greater than that of pillar 1 and pillar 2.

5.4 Stability judgment based on the cusp catastrophe model of local elastic energy rate

The LEER sequence of the key areas are polynomial fitted, they can be obtained as

The whole areas

$$LEER = -5.04x^4 + 741.31x^3 - 9346.6x^2 + 69373x + 32945$$

The trench

$$LEER = -1.96x^4 + 242.74x^3 - 2292x^2 + 17506x + 24572$$

The roof

$$LEER = 3.28x^4\text{-}49.51x^3 + 1533.8x^2\text{-}2417.7x + 13403$$

The pillar 1

$$LEER = \text{-}1.92x^4 + 130.05x^3\text{-}1061.6x^2 + 2639.5x + 5964$$

The pillar 2

$$LEER = 2.96x^4\text{-}92.93x^3 + 1437.8x^2\text{-}8698.8x + 9607.3$$

All the coefficients a_i and the control variables are calculated, and the discrimination value can be obtained. The results are shown in the Table 2.

It can be known from the Table 2 that the final cusp catastrophe discriminant value of whole is bigger than 0 after formation of the three gobs which means the gob system is relative stable. The discrimination value of pillar 2 is the smallest and the discrimination value of trench is the biggest.

The histogram of LERR per unit volume of failure rock is shown in Fig. 20. It can be known that the LERR per unit volume of failure rock in the pillar 2 is the biggest that means the damage degree is the greatest, so the stability is the worst.

In order to analyze the energy distribution of the surrounding rock, the cross-section at y=100 m is selected as the research subject to study the distribution contour of LEER which is shown in Fig. 21. As shown in the figure, the red areas represent the LEER values are greater than 0 which means energy gathers here.

It can be seen from the Fig. 21 that the LEER represents significant partition phenomenon. The LERR distribution shows that there are main energy releases in the horizontal direction and energy concentrations in the vertical direction. There is a large area of energy release in the area above the gobs and the trench areas and a mixing zone of energy release and accumulation in the roof of the middle gob.

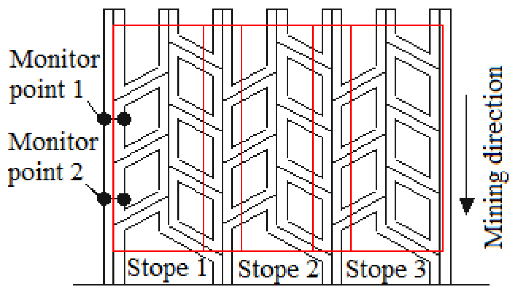

(a)Layout of monitoring points

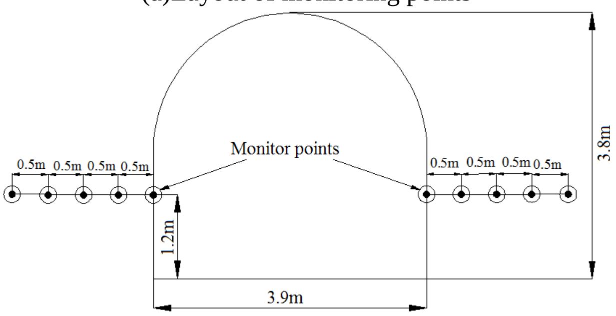

(b) Installation of multi point displacement meter

Fig. 22 Layout of monitoring points

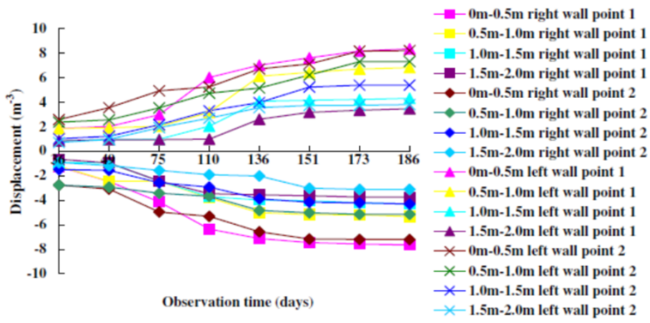

Fig. 23 Displacement curve of monitoring point 1

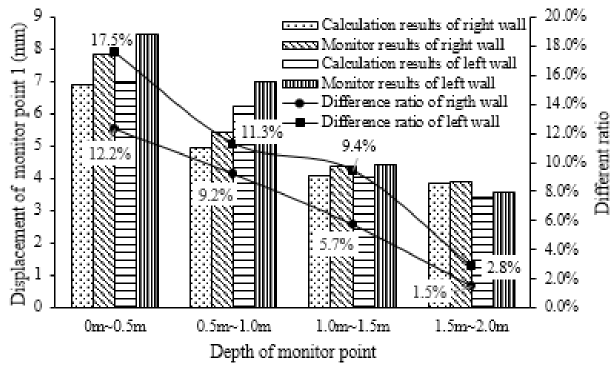

(a) Displacement of monitor point 1

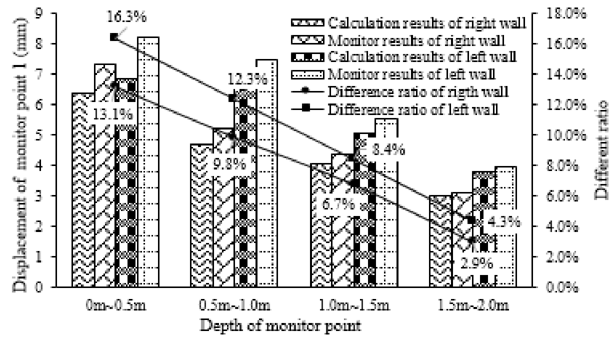

(b) Displacement of monitor point 2

Fig. 24 Comparison of numerical simulation and field monitoring

6. Contrasting calculation results and monitoring data

In the mining process, the JSS30A-10 multi-point extensometers were arranged in the bottom roadway of the stope on the -447.5 m level, which manufactured by Bsida Instrument company, China, having a measuring range of 0.5-30 m with precision 0.1 mm, and they were used to monitor the deformation on the excavation surface as well as at interior points of the two walls of the tunnel as shown in Fig. 22.

Along the roadway axis direction (y-direction), monitoring was conducted at two locations (points 1 and 2). All the deformation data were monitored. The total monitoring duration was 186 days before extracting the ore from the monitoring area. The obtained results are shown in Fig. 23.

As expected intuitively, for each wall and each monitoring point, the highest deformation has occurred at the excavation surface and it has reduced as the monitoring point goes more and more into the rock mass. Point 1 measurements compare quite well with point 2 measurements. Also, a good comparison can be seen between the right wall and left wall measurements.

Fig. 23 shows a comparison between field deformation monitoring results and different numerical analyses results. Overall, the monitored field deformations compare very well with the calculation results shown in Fig. 24. The calculation results are all less than that of monitored field deformations, and the difference ratios between calculation results and monitored field deformations of left wall are all greater than that of right wall. The difference ratios gradually decrease with the increase of depth of monitor points.

A perfect agreement can be obtained between the field values and numerical calculations when the depth is greater than 1.5 m, which means that the model established in this paper and the parameters are much reasonable.

7. Conclusions

(1) The formation of gob in the deep mine is a complex stress adjustment process which includes loading and unloading. The numerical simulation of stability analysis of gob in deep mine often only considers loading stress path which is not consistent with the stress actual conditions of deep mine. The numerical model of gob stability under unloading stress path is established which considers the actual stress conditions. It can provide valuable references for the stability analysis of the deep gob.

(2) For many years, it has been understood that energy changes occur in the rock mass during mining. Therefore, the stability of stope was analyzed based on energy in our paper. Under the effect of high stress, a great deal of elastic energy gathers in the rock internal. During the formation of gob, it is bound to cause massive energy release which may result in failure of rock. The traditional stress and strain indexes do not meet the needs of stability analysis of deep gob. This paper presents the local energy release rate index (LERR) and combines it with the numerical model of unloading. The engineering application results are very well, and it improves the accuracy of stability analysis. It provides a reliable indicator for the stability analysis of gob in the deep mines.

(3) The related researches show that the rock stability is closely related to the overall energy release and distribution of plastic zone. However, the results of this paper show that the total volume of the plastic zone or the overall energy release in a region are the largest, but the corresponding stability is not the worst. Therefore, we should comprehensively consider the energy release cases of failure rock elements. The LERR index can reflect the energy evolution of failure rock which includes the accumulation, and release of energy. Thus, it is particularly suitable for the stability analysis of gob in the deep mine.

(4) In order to simplify the analysis difficulty, the Mohr-Coulomb model is used in this paper. The model cannot reflect the softening behavior, which causes one can't find any seismic energy. Hence, the dissipated energy is not considered. This will be taken into account in the further research.

Acknowledgements

Financial supports for this work, provided by the National Natural Science Foundation of China (No. 5137403), General Financial Grant from the China Postdoctoral Science Foundation (No. 2016M591080) and Fundamental Research Funds for the Central Universities (No. FRF-TP-17-025A2) are gratefully acknowledged. Finally, the first author would like to thank colleagues at USTB for their support.

References

An, B., Zhang, J. and Li, M. (2016), “Stability of pillars in backfilling mining working face to recover room mining standing pillars”, *J. Min. Safe. Eng.*, **33**, 238-245.

Anon. (1986), “Coal mining technology: Some british developments”, *Coal Min.*, **23**(3), 38-40.

Cao, S.G., Zhou, X. and Xie, B. (2009), *Mine Safety Terms*, Standards Press of China, Beijing, China.

Chen, L. (2006), “A study of physical model-test technology and application in Geotechnical Engineering”, Ph.D. Dissertation, Wuhan Institute of Rock and Soil Mechanics, Wuhan, China.

Chen, Z. Hou, K. and Yang, B. (2010), “3D finite element numerical on gob stability of some mine”, *Nonferr. Metal*, **62**(3), 142-145.

Dong, P. (2012), “Study on the impacting effect of roof stopping ore and rock based on discrete element numerical simulation technique”, *Min. Explor.*, **5**, 28.

Feng, Q. and Jiang, B. (2015), “Analytical solution for stress and deformation of the mining floor based on integral transform”, *J. Min. Sci. Technol.*, **25**(4), 581-586.

Gong, F.Q., Li, X.B., Dong, L.J. and Liu, X.L. (2008), “Underground goaf risk evaluation based on uncertainty measurement theory”, *Chin. J. Rock Mech. Eng.*, **27**(2), 323-330.

Hancock, G.R. (2004), “The use of landscape evolution models in mining rehabilitation design”, *Environ. Geol.*, **46**(5), 561-573.

He, G.L., Li, D.C., Zhai, Z.W. and Tang, G.Y. (2007), “Analysis of instability of coal pillar and stiff roof system”, *J. Chin. Coal Soc.*, **32**(9), 897-901.

Hoek, E. and Brown, E.T. (1980), *Underground Excavation in Rock*, London Institution of Mining and Metallurgy.

Kripakov, N.P., Sun, M.C. and Donato, D.A. (1995), “ADNIA applied toward simulation of progressive failure in underground mine structure”, *Comput. Struct.*, **56**(2-3), 329-344.

Lai, X.P., Zhang, L.J. and Cai, M.F. (2003), “Application of neural network to the statistics and prediction of dynamical damage and evolutement in the large scale mine-out area supported by rock based composite materials”, *J. Univ. Sci. Technol. Beijing*, **25**(4), 300-303.

Li, D., Zhao, F. and Zheng, M. (2014), “Fractal characteristics of cracks and fragments generated in unloading rock burst tests”, *J. Min. Sci. Technol.*, **24**(6), 819-823.

Ma, H., Wang, J. and Wang, Y. (2012), “Study on mechanics and domino effect of large-scale goaf cave-in”, *Safe. Sci.*, **50**(4), 689-694.

Mamtimin, G.E.N.I. and Rahmatjian, I. (2014), “Modern numerical simulation methods and its practical applications in engineering”, *Eng. Mech.*, **33**, 11-18.

Mote, C.D. (1971), “Global-local finite element”, *J. Numer.*

Meth. *Eng*., **3**(4), 565-574.

Okada, H., Endoh, S. and Kikuchi, M. (2005), "On fracture analysis using an element overlay technique", *Eng*. *Fract*. *Mech*., **72**(5), 773-789.

Ouria, A., Toufigh, V., Desai, C., Toufigh, V. and Saadatmanesh, H. (2016), "Finite element analysis of a CFRP reinforced retaining wall", *Geomech*. *Eng*., **10**(6), 757-774.

Please, C.P., Mason, D.P., Khalique, C.M., Ngnotchouye, J.M.T., Hutchinson, A.J., van der Merwe, J.N. and Yilmaz, H. (2013), "Fracturing of a Euler-Bernoulli beam in coal mine pillar extraction", *J*. *Rock Mech*. *Min*. *Sci*., **64**, 132-138.

Sakamoto, A., Yamada, N., Iwaki, K. and Kawamoto, T. (2005), "Applicability of recycling materials to cavity filling materials", *J*. *Soc*. *Mater*. *Sci*., **54**(11), 1123-1128.

Shang, Z., Tang, S. and Jiao, W. (2014), "Failure probability of goaf in large-scale based on simulation of FLAC^{3D}", *Rock Soil Mech*., **35**, 3000-3006.

Shreedharan, S. and Kulatilake, P.H. (2016), "Discontinuum-equivalent continuum analysis of the stability of tunnels in a deep coal mine using the distinct element method", *Rock Mech*. *Rock Eng*., **49**(5), 1903-1922.

Song, W.D., Fu, J.X., Du, J.H. and Zhang, C.L. (2012), "Analysis of stability of goaf group in metal mines based on precision detection", *Rock Soil Mech*., **33**(12), 3781-3787.

Tang, L., Zhou, J. and Zhang, J. (2012), "Mechanical response of deep stope-out areas and filling effect under dynamic disturbance", *J*. *Chengdu Univ*. *Technol*., **39**(6), 623-628.

Tao, M., Chen, Z., Li, X., Zhao, H. and Yin, T. (2016), "Theoretical and numerical analysis of the influence of initial stress gradient on wave propagations", *Geomech*. *Eng*., **10**(3), 285-296.

Terada, K. and Kikuchi, N. (2001), "A class of general algorithms for multi-scale analyses of heterogeneous media", *Comput*. *Meth*. *Appl*. *Mech*. *Eng*., **190**(40-41), 5427-5464.

Tulu, I.B. and Heasley, K.A. (2011), "Investigating the mechanics of pillar loading through the analysis of in-situ stress measurements", *Proceedings of the 45th US Rock Mechanics/Geomechanics Symposium*, San Francisco, California, U.S.A., June.

Wang, C., Guo, J. and Wang, L. (2015), "Recognition of goaf risk based on support vector machines method", *J*. *Chongqing Univ*., **38**, 85-93.

Wang, H., Li, Y., Li, S., Zhang, Q. and Liu, J. (2016), "An elasto-plastic damage constitutive model for jointed rock mass with an application", *Geomech*. *Eng*., **11**(1), 77-94.

Wang, X., Kulatilake, P.H.S.W. and Song, W.D. (2011), "Stability investigations around a mine tunnel through three-dimensional discontinuum and continuum stress analyses", *Tunn*. *Undergr*. *Sp*. *Technol*., **32**, 98-112.

Whittles, D.N., Lowndes, I.S., Kingman, S., Yates, C. and Jobling, S. (2007), "The stability of methane capture boreholes around a long wall coal panel", *J*. *Coal Geol*., **71**(2-3), 313-328.

Wu, Y., Zhang, X. and Li, X. (2010), "Discrete element simulation of collapse of mined-out area", *Min*. *Technol*., **2901**, 73-80.

Yu, B., Zhang, Z., Kuang, T. and Liu, J. (2016), "Stress changes and deformation monitoring of longwall coal pillars located in weak ground", *Rock Mech*. *Rock Eng*., **49**(8), 3293-3305.

Zhang, Y.P., Cao, P., Yuan, H.P. and Dong, L.J. (2010), "Numerical simulation on stability of complicated goaf", *J*. *Min*. *Safe*. *Eng*., **27**(2), 233-238.

CC